Back to Table of Contents

TRANSMISSION LINE PROTECTION SYSTEM FOR INCREASING POWER SYSTEM REQUIREMENTS

ARMANDO GUZMÁN, JOE MOONEY,
GABRIEL BENMOUYAL, NORMANN FISCHER

SCHWEITZER ENGINEERING LABORATORIES, INC.
PULLMAN, WASHINGTON USA

Presented before the

29th ANNUAL
WESTERN PROTECTIVE RELAY CONFERENCE
SPOKANE, WASHINGTON
OCTOBER 22–24, 2002

TRANSMISSION LINE PROTECTION SYSTEM FOR INCREASING POWER SYSTEM REQUIREMENTS

Armando Guzmán, Joe Mooney, Gabriel Benmouyal, Normann Fischer
Schweitzer Engineering Laboratories, Inc.
Pullman, WA USA

ABSTRACT

This paper describes a protective relay for fast and reliable transmission line protection that combines elements that respond only to transient conditions with elements that respond to transient and steady state conditions. In this paper, we also present an algorithm that prevents Zone 1 distance element overreach in series-compensated line applications and show how to prevent corruption of the distance element polarization during pole-open conditions. We also introduce an efficient frequency estimation logic for single-pole-tripping (SPT) applications with line-side potentials. This logic prevents distance element misoperation during a system frequency excursion when one pole is open. We also discuss an algorithm and logic to prevent single-pole reclosing while the fault is present, avoiding additional power system damage and minimizing system disturbance. Applying these algorithms and logics results in a protective system suitable for increasing power system requirements such as heavy loading, SPT, series line compensation, and shunt line compensation.

INTRODUCTION

Right-of-way restrictions and limitations on building new transmission lines necessitate optimization of transmission networks. This optimization imposes challenges on distance relay-based transmission line protection. Network optimization increases transmission line loading and requires fast fault clearing times because of reduced stability margins.

In many cases, series compensation, SPT, or the combination of both is necessary to optimize transmission network investment. Series compensation generates subharmonics that can cause distance element overreach. SPT adds complexity to the ability of the distance element to track the power system frequency during single-pole open (SPO) conditions when the line protection uses line-side potentials.

Shunt compensation can corrupt the distance element polarization because of the presence of transient voltages during three-pole open conditions when the line protection uses line-side potentials.

SPT applications without arc extinction methods can jeopardize power system operation if the fault condition has not disappeared before the reclosing attempt; that is, the breaker closes under fault condition, making the power system prone to instability.

Combining elements that respond only to transient conditions with elements that respond to transient and steady state conditions results in dependable, high-speed protection. Dedicated logic for series compensation applications adds security to the distance elements in the presence of subharmonics. Flexible polarizing quantities and frequency tracking algorithms adapt to different breaker and system operating conditions. Secondary arc extinction detection optimizes the single-pole open interval and minimizes power system damage in SPT applications.

In this paper, we present solutions to the above issues that result in improved transmission line protection suitable for the most challenging power system requirements.

RELIABLE HIGH-SPEED TRIPPING

A significant reduction in operating time is one trend in recently developed digital transmission line relays. A number of new techniques allow secure sub-cycle tripping of transmission line distance relays. One of the first proposed methods uses variable-length data-window filtering with adaptive zone reach [1]. Developments described in Reference [2] introduced the concept of multiple data-window filters (a total of four) with corresponding fixed reach (the smaller the data-window, the smaller the reach). Line protective relays not only need to pick up fast for incipient faults but also to provide proper and fast fault type selection in SPT applications.

High-Speed Distance Element Operating Principles

Based on the principle of multiple data-window filters mentioned above [2], we developed the concept of the dual-filter scheme. This scheme combines voltage and current data from half-cycle and one-cycle windows (Figure 1) to obtain Zone 1 distance element detection and achieve fast tripping times.

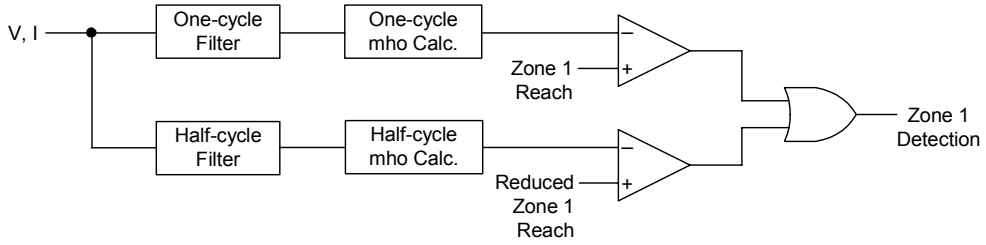

Figure 1 Concept of a Zone 1 Distance Element Using Dual-Filter Scheme

The mho calculation in Figure 1 uses operating (S_{OP}) and polarizing (S_{POL}) vector quantities defined as follows to implement mho distance element calculations [3]:

$$S_{OP} = r \cdot Z_{L1} \cdot I_R - V_R \quad \text{Equation 1}$$

$$S_{POL} = V_{POL} \quad \text{Equation 2}$$

Where,

- V_R = line voltage of the corresponding impedance loop
- I_R = line current of the corresponding impedance loop
- Z_{L1} = positive-sequence line impedance
- r = per-unit mho element reach
- V_{POL} = polarizing voltage

V_R and I_R are the relay voltage and current phasors particular to an impedance loop (six loops are necessary to detect all faults), and V_{POL} is the polarizing voltage, consisting of the memorized positive-sequence phasor [3]. A mho element with reach r detects the fault when the scalar product between the two vectors is positive (i.e., the angle difference between S_{OP} and S_{POL} is less than 90 degrees). We can represent this condition mathematically as:

$$\mathrm{Real}\left[\left(r \cdot Z_{L1} \cdot I_R - V_R\right) \cdot V_{POL}^{*}\right] \geq 0 \quad \text{Equation 3}$$

In this expression, "Real" stands for "real part of" and "*" for "complex conjugate of."

For a forward fault, this expression becomes equivalent to the reach r being greater than a distance m computed in Equation 4 [3]:

$$r \cdot |Z_{L1}| \geq m \cdot |Z_{L1}| = \frac{Real\left[V_R \cdot V_{POL}^*\right]}{Real\left[\left(1\angle\theta_{L1}\right) \cdot I_R \cdot V_{POL}^*\right]} \qquad \text{Equation 4}$$

Where,

$1\angle\theta_{L1}$ = phasor with unity magnitude and an angle equal to the positive-sequence line impedance angle
m = per-unit distance to fault

As Figure 1 shows, we use two sets of filtering systems to achieve speed in fault detection: one fast (data window of one half-cycle) and one conventional (data window of one-cycle) to compute the line voltage and current phasors. For each loop, we implement two mho-type detectors, each of which uses the fast or the conventional phasors. We achieve the final detection logic simply by "ORing" the outputs from the two mho-type detectors. We apply this principle for Zone 1 detection and for zones (normally 2 and 3) used in communications-assisted schemes (POTT, DCB, etc.). In the case of Zone 1, the half-cycle detector has a reach less than the one-cycle detector reach. For Zones 2 and 3, the reach remains the same. We do not apply the principle in time-delayed stepped distance schemes because high-speed detection offers no benefit with the delayed outputs of these schemes. For each zone and the corresponding six impedance loops, using the two sets of phasors to implement two calculations for the distance m leads necessarily to a faster result with the phasors derived from the half-cycle window than with phasors derived from the one-cycle window.

Mho-type detectors are inherently directional but are not useful for fault type selection because multiple elements pick up for single-phase-to-ground faults. Furthermore, phasors derived from the half-cycle data window are less stable than the ones derived with a one-cycle data window. Therefore, in order to achieve security for high-speed tripping, we supplement the fast mho-type fault detectors with an algorithm called High-Speed Directional and Fault Type Selection, HSD-FTS [4][5]. This algorithm calculates three incremental torques (Equation 5) to determine the faulted phases and the fault direction.

$$\begin{aligned} \Delta T_{AB} &= Real\left[\Delta V_{AB} \cdot \left(1\angle\theta_{L1} \cdot \Delta I_{AB}\right)^*\right] \\ \Delta T_{BC} &= Real\left[\Delta V_{BC} \cdot \left(1\angle\theta_{L1} \cdot \Delta I_{BC}\right)^*\right] \\ \Delta T_{CA} &= Real\left[\Delta V_{CA} \cdot \left(1\angle\theta_{L1} \cdot \Delta I_{CA}\right)^*\right] \end{aligned} \qquad \text{Equation 5}$$

Where,

ΔV_{AB} = two-cycle window incremental A-phase-to-B-phase voltage
ΔI_{AB} = two-cycle window incremental A-phase-to-B-phase current

The relay uses the sign of the torques to establish direction and the relative values of these torques to select fault type. The high-speed directional element, HSD, provides a combined directional and fault type selection signal for a total of seven outputs in each direction; Table 1 shows the elements for forward faults (equivalent elements are derived for reverse faults). As shown in Table 1, we use a logical "AND" to combine each fast mho element with the corresponding HSD-FTS output. The result of this combination has two objectives:

- Provide a single output when a fault detection occurs, allowing then reliable fault type selection for SPT applications.
- Provide fast and reliable fault detection, allowing fast tripping times.

Table 1 Combining the HSD-FTS and Fast Mho Element Logic

HSD-FTS Output	Fault Type Selection	"ANDed" With
HSD-AGF	Forward A-phase-to-ground	MHO-AGH
HSD-BGF	Forward B-phase-to-ground	MHO-BGH
HSD-CGF	Forward C-phase-to-ground	MHO-CGH
HSD-ABF	Forward phases A-B	MHO-ABH
HSD-BCF	Forward phases B-C	MHO-BCH
HSD-CAF	Forward phases C-A	MHO-CAH
HSD-ABCF	Forward phases A-B-C	MHO-ABH, MHO-BCH, MHO-CAH

As shown in Figure 2 in the case of the A-phase-to-ground impedance loop, we simply "OR" signals from the one-cycle and half-cycle data-window fault detectors to get the final loop logic signal. We apply similar logic for the five other impedance loops. Note that we also supplement the conventional one-cycle mho element with a directional element [6] derived from the one-cycle data window and with a fault type selection logic [3].

The result of this technique is that reliable high-speed fault detection occurs before conventional one-cycle fault detection. The amount of time advance varies and depends primarily upon the network (particularly the source-impedance ratio, SIR) and the fault location. Extensive testing revealed that fault detection occurs in practically all cases within a sub-cycle time frame.

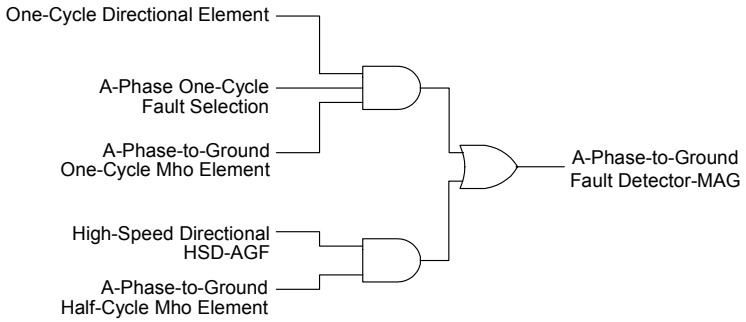

Figure 2 A-Phase Impedance Loop Half- and One-Cycle Combination Logic

High-Speed Distance Element Performance

As an example, Figure 3 shows the two calculations of the distance m for a long line (in a 50 Hz system), Zone 2 A-phase-to-ground fault occurring at 0.1 s in a system with an SIR = 0.2. In this case, the half-cycle signal detects the fault at 0.111 s and the one-cycle signal detects the fault at 0.123 s. The half-cycle element detects the fault 12 ms faster than the one-cycle element.

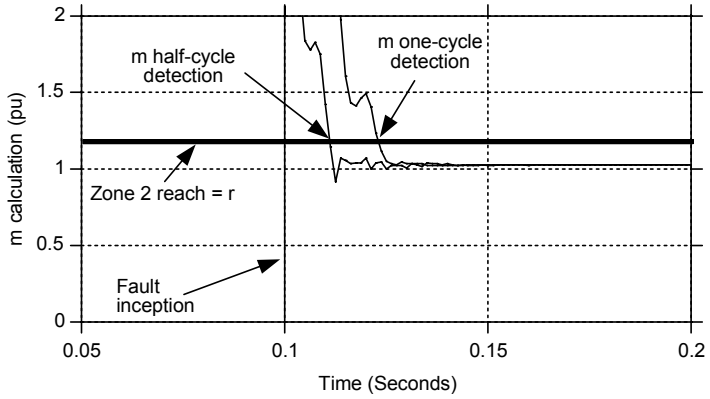

Figure 3 m Calculations for a Zone 2 A-Phase-to-Ground Fault

For the same example as the Zone 2 A-phase-to-ground fault shown in Figure 3, the timing of the different half-cycle and one-cycle signals is shown in Figure 4. The HSD-FTS signal (HSD-AGF in this case) occurs first (this signal has a duration of two cycles because it is based on superimposed quantities). After a few milliseconds, the half-cycle mho element (MHO-AGH) follows. More than a half-cycle later, we have the one-cycle mho (MHO-AGF) detection.

Because the mho-detector signals are "ORed", the time occurrence of the final fault detection MHO-AG corresponds to the fast detection MHO-AGH. In this case, we achieve an improvement, typical in practically all cases, of about one half-cycle. Two cycles after the fault inception, the detection depends only upon the one-cycle derived signals.

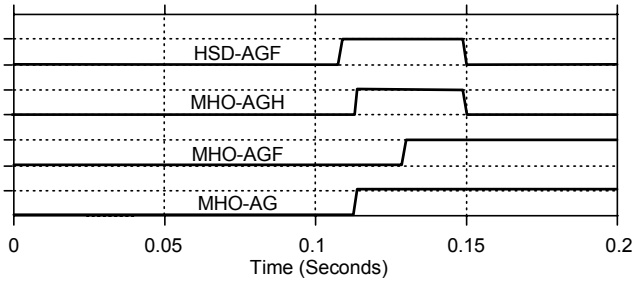

Figure 4 A-Phase-to-Ground Zone 2 Fault Signals

SERIES COMPENSATION OVERREACHING PROBLEMS AND SOLUTION

Series capacitors applied on transmission systems improve system stability and increase power transfer capability. The application of a series capacitor reduces the inductive reactance of the given transmission line, making the line appear electrically shorter. Although series capacitors may improve power system operation, using these capacitors results in a challenging problem for impedance-based line protection.

Adding series capacitors on a transmission line causes subharmonic transients to occur following faults or switching of the series capacitor. These subharmonics can cause underreaching Zone 1 distance elements to overreach for external faults. There are other problems associated with subsynchronous resonance in generators. In this paper, we focus on problems associated with distance relays.

All series capacitors come equipped with protective elements that reduce or eliminate over-voltages across the capacitor. The protection may be as simple as a spark gap set to flashover at a given voltage or as elaborate as metal-oxide varistors (MOV) using complex energy monitoring schemes. In any case, operation of the series capacitor protection elements can either remove the series capacitor completely or change capacitive reactance in a nonlinear fashion.

The simplest series capacitor protection scheme removes the series capacitor when the series capacitor voltage exceeds a set threshold. The use of a spark gap protection scheme can simplify use of underreaching distance relays on series-compensated lines. Firing of the spark gap for external faults may prevent Zone 1 overreach, so it is then possible to ignore the series capacitor. In most applications, however, the spark gap firing voltage threshold is high enough that the spark gap does not fire for external faults.

MOVs present an interesting challenge because this type of protection scheme does not fully remove the series capacitor. In fact, the capacitive reactance can be very nonlinear. We can use an iterative model [16] to approximate the effective reactance of the MOV-protected bank. However, this model does not provide insight about the transient response. Some MOV-protected capacitor banks include energy monitoring of the MOVs. Bypassing of the capacitor bank occurs when the energy level exceeds a specified threshold. This can work to our advantage when we use impedance-based schemes.

In either case, we need careful analysis and study before applying any impedance-based protection scheme on series-compensated lines.

Distance Relay Overreaching Problems

The series connection of the capacitor, the transmission line, and the system source create a resonant RLC circuit. The natural frequency of the circuit is a function of the level of compensation and the equivalent power system source. The level of compensation can change according to the switching in and out of series capacitor "segments." The source impedance can change because of switching operations external to the protected line section.

Figure 5 illustrates a transmission line with a 50 percent series-compensated system (e.g., the series capacitor reactance equals 50 percent of the positive-sequence line reactance). For the fault location shown, the underreaching distance element at the remote terminal (Station S) should not operate. Intuitively, we would expect that setting the reach to 80 percent of the compensated impedance ($Z_{L1} - jX_C$) would be an appropriate reach setting. However, the series capacitor and the system inductance generate subharmonic oscillations that can cause severe overreach of the distance element. Figure 6 shows the impedance plane plot for the fault location shown in Figure 5 (where the series capacitor remains in service).

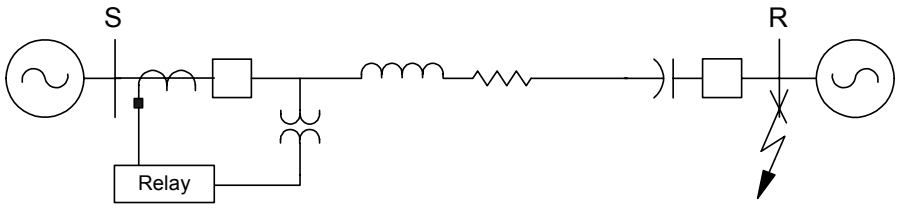

Figure 5 System With Series Capacitors at One End With a Fault at the End of the Line

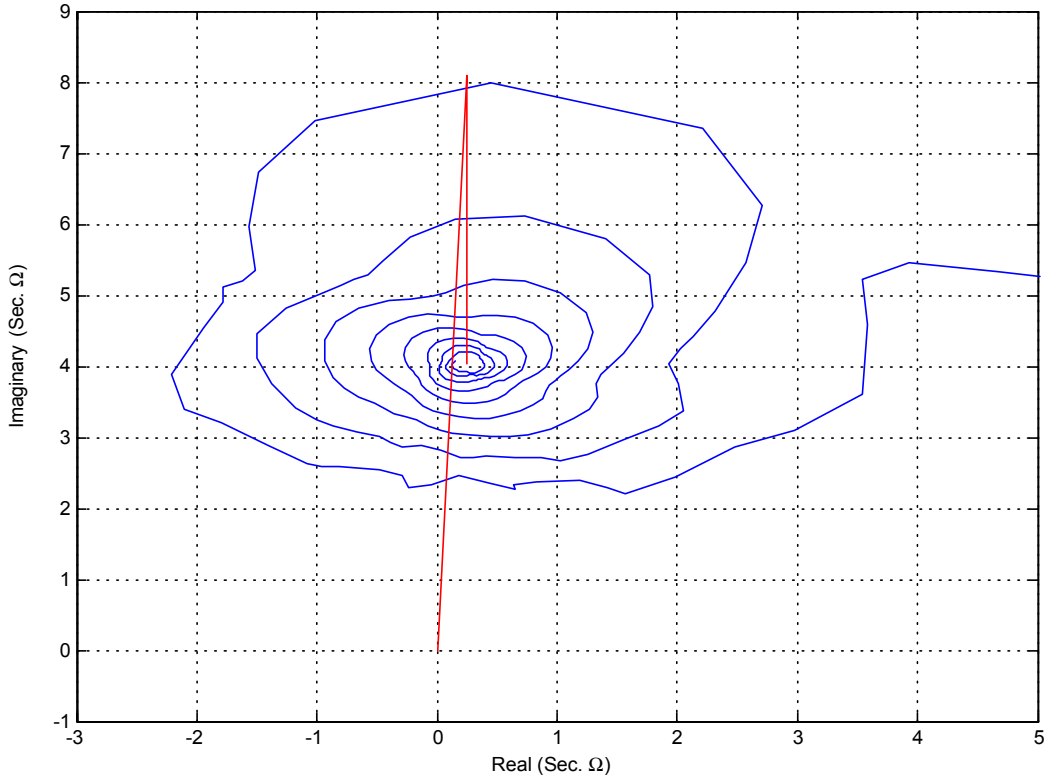

Figure 6 Apparent Impedance for a Fault at the End of the Line

As we can see from the impedance plot, the apparent impedance magnitude decreases to a value as low as 2 ohms secondary. This value is close to half of the compensated line impedance! Note that in Figure 6 the capacitor is modeled with no overvoltage protection. This condition is common for most external faults, because the overvoltage protection is typically sized to accommodate external faults (e.g., the overvoltage protection does not operate for external faults).

Scheme to Prevent Distance Element Overreach (Patent Pending)

From Figure 5, we can calculate the voltage drop for a bolted A-phase-to-ground fault at the line end as follows:

$$V_{CALC} = \left| \left[\left(I_A + k_0 \cdot I_G \right) \cdot Z_{L1} \right] + \left[I_A \cdot \left(-jX_C \right) \right] \right| \qquad \text{Equation 6}$$

Where:

I_A = A-phase current at the relay location
I_G = residual or ground current at the relay location
k_0 = zero-sequence compensation factor
Z_{L1} = positive-sequence line impedance
X_C = capacitive reactance that the relay "sees"

Ignoring variables such as mutual coupling and fault resistance, we can see that the calculated voltage equals the measured voltage. Determining the ratio of the measured voltage to the calculated voltage would result in unity or one.

When the fault moves to the other side of the series capacitor (line-side), the measured voltage increases and the calculated voltage decreases. The measured voltage increases because the series capacitor is no longer between the relay and the fault, and the line appears to be electrically longer. The calculated voltage decreases because the calculated voltage always includes the series capacitor. The ratio of the measured voltage to the calculated voltage is greater than one for a fault at this location.

As the fault nears the relay location, the measured voltage decreases and the calculated voltage increases. The ratio of the measured voltage to the calculated voltage approaches zero as the fault location nears the relay location. Figure 7 is a plot of the measured voltage, V_{MEAS}, calculated voltage, V_{CALC}, and the ratio of the measured to the calculated voltage. Note that the scale is arbitrary; the purpose of this figure is to illustrate how the voltage magnitudes and the voltage ratio change with respect to fault location.

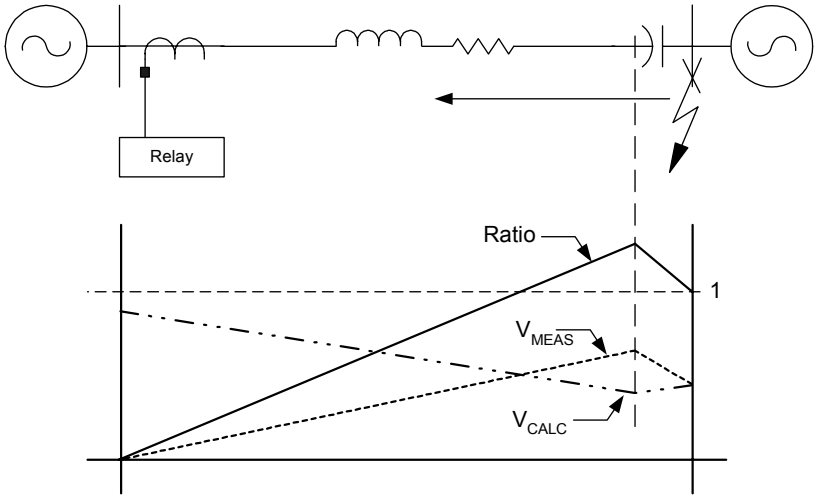

Figure 7 Measured and Calculated Voltages and Voltage Ratio for Faults Along the Line

We can use the ratio we described earlier to supervise underreaching Zone 1 distance elements to prevent overreach for external faults. When the ratio of the measured to calculated voltage is less than a pre-defined threshold, the Zone 1 distance element can operate. Otherwise, the Zone 1 element is blocked. The only additional information that the relay needs to calculate this ratio is the capacitive reactance that the relay "sees." With the ratio supervision, you can set the Zone 1 reach based on the uncompensated line impedance.

DISTANCE ELEMENT POLARIZATION DURING POLE-OPEN CONDITIONS

V_{POL} is the polarizing voltage for calculating the distance to fault, m, as Equation 4 illustrates. The most popular polarizing quantity for distance protection is positive-sequence voltage with memory [2]. During pole-open conditions in applications with line-side potentials, eventual corruption of the polarizing quantity can occur if the input voltage to the memory circuit is corrupted. Invalid memory polarization may cause distance element misoperation. Shunt reactor switching generates damped oscillations with signals that have frequencies different from the actual system frequency. Let us look at an example of these signals and the logic that prevents the memory polarization from using unhealthy voltages.

Shunt Reactor Switching

Shunt reactors compensate the line charging currents and reduce overvoltages in long transmission lines. Figure 8 shows a 735 kV transmission line with shunt compensation at both ends of the line, 200 MVARs at each line end. The figure also shows line capacitance that generates 546 MVARs of reactive power. After the circuit breakers open at both line ends, the remaining circuit is basically an RLC circuit with a natural frequency of about 51.36 Hz; the circuit has stored energy in the reactor and in the line capacitance. Note that the circuit natural frequency is close to the nominal system frequency of 60 Hz. After the three poles of each line breaker open, the shunt reactors interact with the line capacitance and maintain line voltages for several cycles. The circuit applies these voltages to the potential transformers (PTs) or capacitive voltage transformers (CVTs). These voltages corrupt the distance protection polarization and frequency estimation. Figure 9 shows the A-phase voltage at the relay location after deenergization of the line (in Figure 8). There is no need to feed this distorted voltage to the distance protection polarization and frequency estimation algorithm, as we explain later.

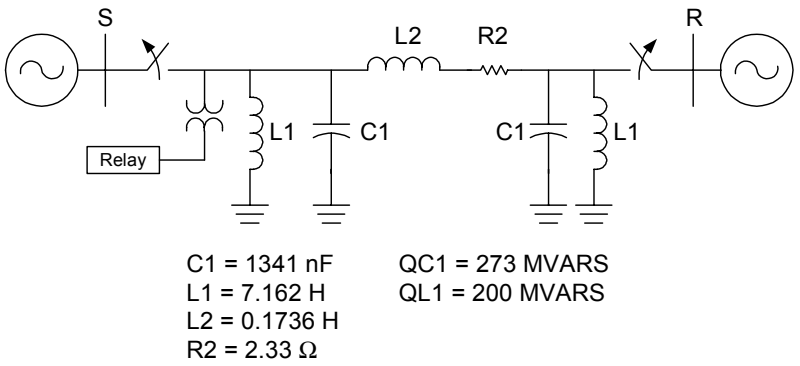

Figure 8 735 kV Transmission Line With Shunt Compensation at Both Ends of the Line

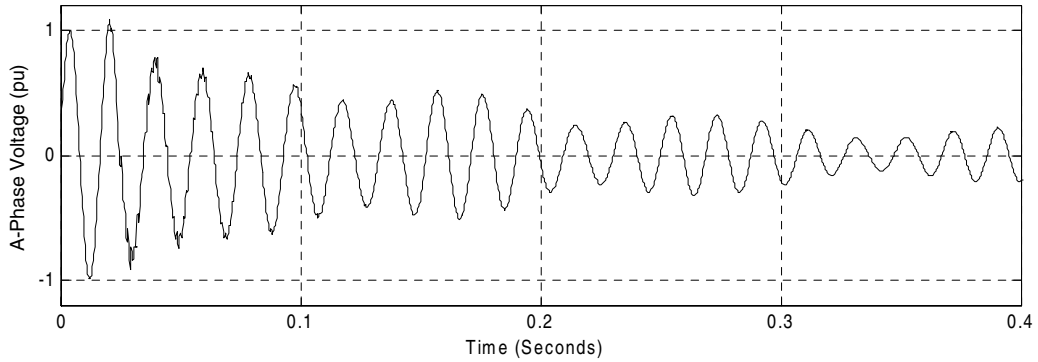

Figure 9 A-Phase Line Voltage After Line Deenergization

Reliable Polarizing Signal During Pole-Open Conditions

We need to eliminate the positive voltage input (V_1) to the polarizing memory when the voltage is distorted. Figure 9 illustrates a voltage ringing condition after the circuit breakers open at both line ends. The relay detects this ringing condition and eliminates the corrupted voltage from the memory filter input. On a phase-by-phase basis, the relay inputs zeros to the memory filter during pole-open conditions to prevent distance element misoperation. Figure 10 shows the logic

for inputting zeros to the memory filter after the relay detects voltage ringing or undervoltage conditions.

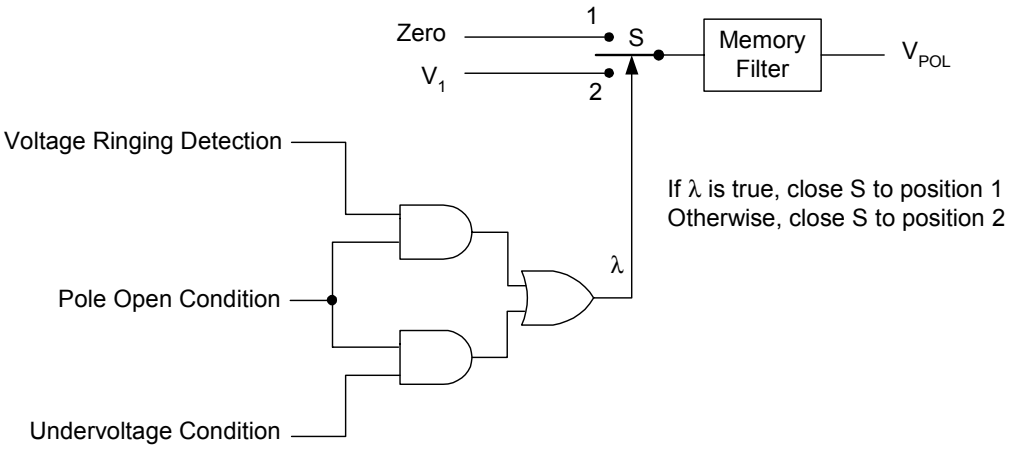

Figure 10 The Relay Inputs Zeros to the Memory Filter When Input Voltages are Corrupted

EFFICIENT FREQUENCY ESTIMATION DURING POLE-OPEN CONDITIONS

Figure 11 shows a two-source system with line protection using line-side potentials in an SPT application. This figure also shows Breaker 1 (BK1) and Breaker 2 (BK2) A-phase open, indicating a single-pole open condition for both breakers. The distance element can misoperate during frequency excursions and single-pole open conditions if it does not track the system frequency correctly [2]. To prevent relay misoperations, the distance element needs a reliable frequency estimation algorithm for proper frequency tracking during breaker pole-open conditions.

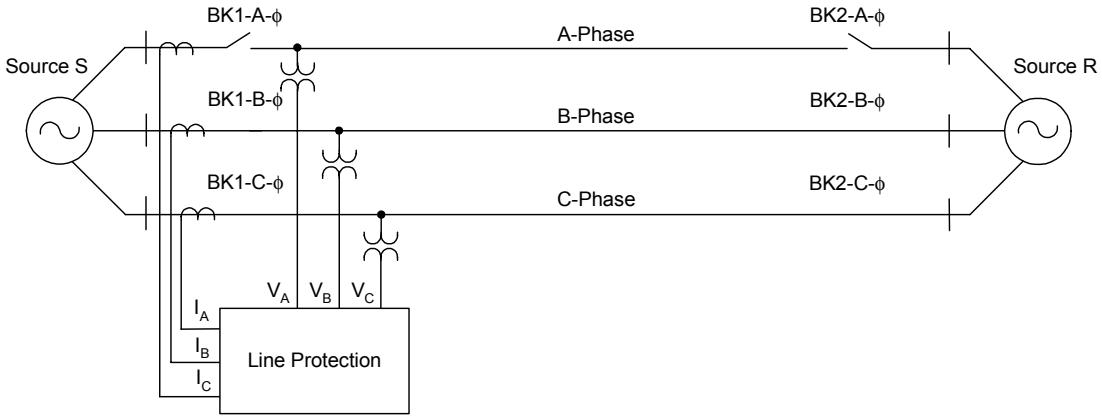

Figure 11 Line Protection Using Line-Side Potential Transformers in a Single-Pole Tripping Application

Traditionally, relays that calculate frequency must have circuitry that detects zero-crossings of the voltage signals to determine the signal period. The inverse of the signal period is the frequency. Normally, this circuitry monitors a single-phase voltage; the relay cannot measure frequency if the monitored phase is deenergized during the pole-open condition. Some numerical relays use zero-crossing detection [7] or rate-of-change of angle algorithms to calculate frequency [8].

Some of these relays use positive-sequence voltage to include voltage information from the three phases [8]. These relays calculate frequency reliably as long as the voltages are present and healthy.

Parallel line mutual coupling [12][13] or line resonance because of shunt reactor compensation can cause voltage distortion during the pole-open condition; this distortion introduces frequency estimation errors. This section describes logic to correctly estimate the system frequency during pole-open conditions and unhealthy voltage conditions.

Frequency Estimation Sources of Error

The following are power system conditions that the frequency estimation logic evaluates to prevent distance element misoperation. First, we show a frequency excursion during a pole-open condition. Second, we show the frequency of the voltage signal after a transmission line deenergization.

Frequency Excursion During Pole-Open Condition

During pole-open conditions, the power system is prone to instability. Particularly in weak source systems, the frequency changes when one phase is open because of the sudden increase in the impedance between the two line terminals. The distance relay needs to track this frequency to minimize distance element overreach. Figure 12 shows a 600 MVA generator connected to a 275 kV network through two transmission lines. The frequency changes, as illustrated in Figure 13, when Line 2 opens A-phase to clear an A-phase-to-ground fault located 50 km from Station S while Line 1 is open. The frequency varies from 60.2 to 59.8 Hz during the pole-open condition.

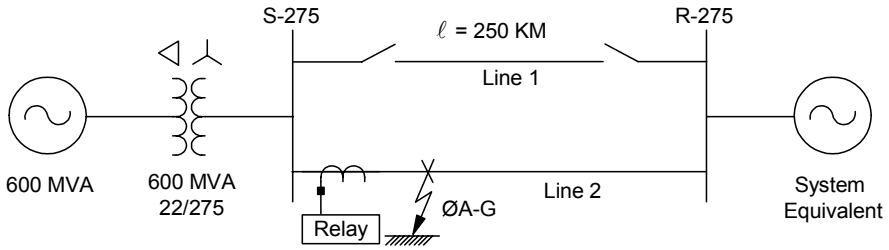

Figure 12 275 kV Network With 600 MVA Generator

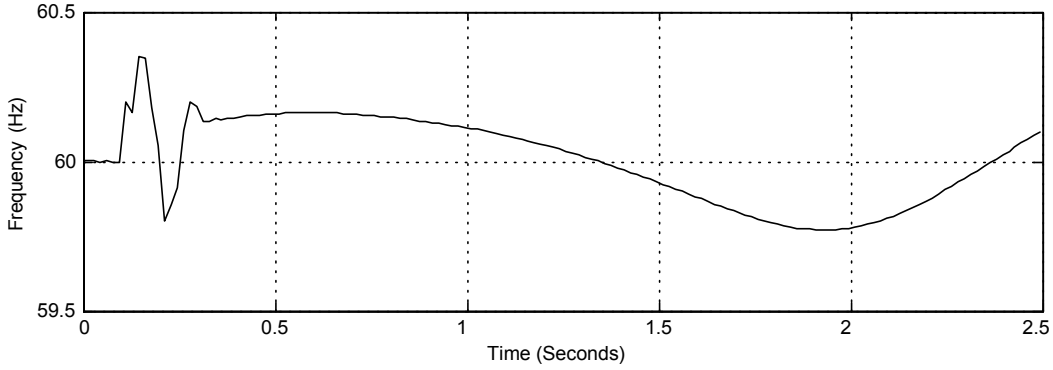

Figure 13 Frequency at the Terminal Close to the 600 MVA Generator

If the relay in Figure 12 does not track the system frequency, the apparent impedance begins to appear as a fault condition, as shown in Figure 14. The relay must use voltage information from the unfaulted phases to track the system frequency and minimize distance element overreach.

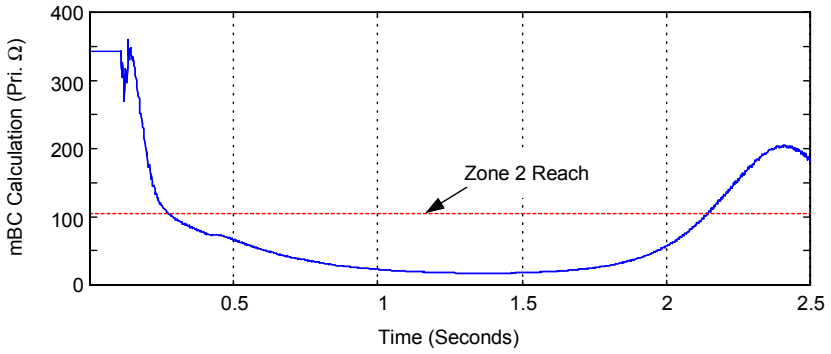

Figure 14 Distance Element Apparent Impedance During Pole-Open Conditions

Shunt Reactor Compensation

We saw earlier the line voltages resulting from the deenergization of a line with shunt reactor compensation. Figure 15 shows the frequency estimation for the A-phase voltage in Figure 9; the frequency of the voltage signal oscillates between 44.6 and 54.4 Hz after the line deenergization (Figure 15). These corrupted voltages must be removed from the frequency estimation logic to prevent errors in the estimation, as we see later.

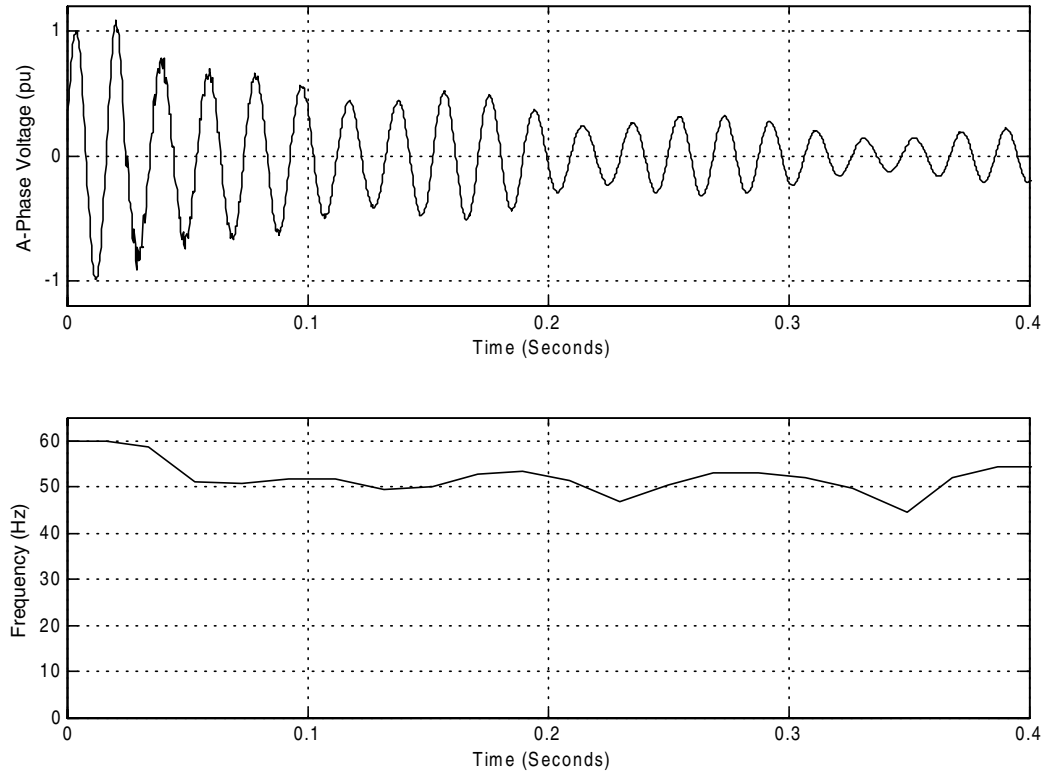

Figure 15 Frequency Estimation Using A-Phase Voltage After Line Denergization

Frequency Estimation Logic (Patent Pending)

Figure 16 shows the logic for frequency estimation that increases distance element reliability. The figure also shows alternate methods for determining the power system frequency, FREQ, for normal system operating conditions, pole-open conditions, and unhealthy voltage conditions. The relay uses FREQ to obtain the relay tracking frequency and to adapt the line protection to power system changes.

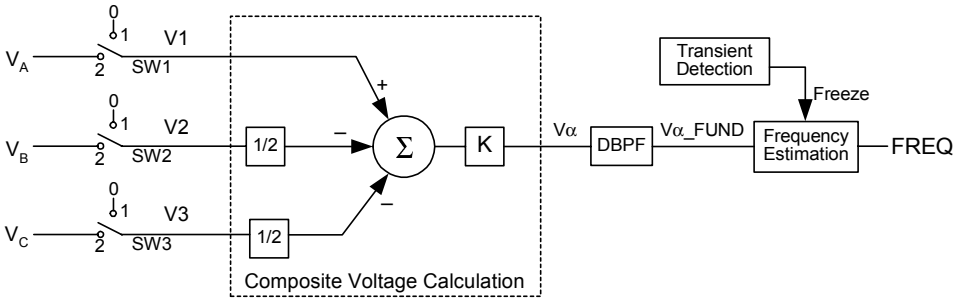

Figure 16 Frequency Estimation Logic for Transmission Line Protection Applications

The relay uses the V_A, V_B, and V_C voltages to calculate the frequency, FREQ. Depending on breaker pole status and voltage source health, switches SW1, SW2, and SW3 select the V_A, V_B, and V_C voltages, respectively, or zero. Switches SW1, SW2, and SW3 have two positions. Position 2 is the normal state; the switches are in this position if the corresponding pole is closed. The relay applies the source voltages when SW1, SW2, and SW3 are in Position 2. The relay selects Position 1 for SW1, SW2, and SW3 according to the following:

- SW1 is in Position 1 when there is an A-phase pole-open, SPOA, condition; a three-pole open, 3PO, condition; or a loss-of-potential (LOP), condition. When SW1 is in Position 1, V1 is zero. Otherwise, V1 = V_A.
- SW2 is in Position 1 when there is a B-phase pole-open, SPOB, condition; a 3PO condition; or an LOP condition. When SW2 is in Position 1, V2 is zero. Otherwise, V2 = V_B.
- SW3 is in Position 1 when there is a C-phase pole-open, SPOC, condition; a 3PO condition; or an LOP condition. When SW3 is in Position 1, V3 is zero. Otherwise, V3 = V_C.

V1, V2, and V3 are the voltages after SW1, SW2, and SW3 switch selection. The relay uses these voltages to calculate the composite signal, V_α [14]. Equation 7 shows the V_α calculation.

$$V_\alpha = \left(V1 - \frac{V2}{2} - \frac{V3}{2} \right) \cdot K \qquad \text{Equation 7}$$

Where the constant K depends on the SW1, SW2, and SW3 switch positions as shown in Table 2.

Table 2 K Constant to Calculate the Composite Voltage,V_α, Depends on Breaker Pole Condition

Breaker Pole Condition			SW1 Position	SW2 Position	SW3 Position	K
A Pole	B Pole	C Pole				
Closed	Closed	Closed	2	2	2	2/3
Open	Closed	Closed	1	2	2	2
Closed	Open	Closed	2	1	2	$2/\sqrt{7}$
Closed	Closed	Open	2	2	1	$2/\sqrt{7}$
Closed	Open	Open	2	1	1	1
Open	Closed	Open	1	2	1	2
Open	Open	Closed	1	1	2	2
Open	Open	Open	1	1	1	2/3

The digital band-pass filter, DBPF, extracts the fundamental component signal (60 Hz or 50 Hz) from the composite voltage, V_α, to obtain V_{α_FUND}. The relay uses the fundamental quantity, V_{α_FUND}, to calculate the frequency, FREQ. As stated before, there are several methods for calculating frequency [7][8][9][10]. In this case, the frequency estimation algorithm uses the zero-crossing detection method. To prevent erroneous frequency estimation during power system transients (faults), the relay freezes the output of the frequency estimator if the relay detects a transient or a tripping condition. The output of the logic is the power system frequency, FREQ. The relay uses this frequency to determine the tracking frequency.

The frequency estimation logic removes the voltage signal from the open phase to prevent using corrupted signals during pole-open conditions or LOP conditions. The composite signal, V_α, allows the relay to combine information from three phases without additional signal manipulation with the "a" operator [15], as in the case of positive-sequence quantity. This composite signal does not require additional filtering for implementation and has improved transient response. The relay uses the composite signal, V_α, to track the system frequency during pole-open conditions. The constant K (see Table 2) modifies the gain of the composite signal, V_α, to provide a constant signal amplitude to the frequency estimator for different line operating conditions.

SECONDARY ARC EXTINCTION DETECTION AND ADAPTIVE RECLOSING

One of the challenges in SPT applications is to prevent the breaker pole from reclosing before the fault extinguishes. Reclosing under fault provides added power system damage and compromises system stability. There are several approaches to prevent these damaging conditions. One of the most common approaches is to add shunt and neutral reactors [17] to suppress the secondary arc present during the pole-open condition and have a dead time (open phase interval) long enough to allow for arc suppression and air de-ionization. Another approach is to increase the dead time and expect the secondary arc to be self-extinguished. None of these approaches verify expiration of the arc before the breaker pole recloses.

As soon as the arc extinguishes, recovery voltage appears across the secondary arc path. This recovery voltage may initiate a restrike and create a reclose-onto-fault condition. Ideally, we want the breaker to close if and only if there is no fault on the line. Detection of the secondary arc extinction prevents reclosing under fault conditions and optimizes the dead time.

The Secondary Arc Phenomenon

In a three-phase circuit, there is electromagnetic and electrostatic coupling between the phase conductors [11]. A phase-to-ground fault results in formation of a primary arc between the faulted phase and ground. A protective system isolates the faulted phase from the power system in SPT applications; the other two healthy phases remain in service, thereby isolating the primary arc. Because two of the three phases are still at approximately nominal voltage and the faulted phase is coupled capacitively and inductively to the healthy phases, a secondary arc is maintained. The air is already ionized from the primary fault, so the two healthy phases need little current to maintain this secondary arc.

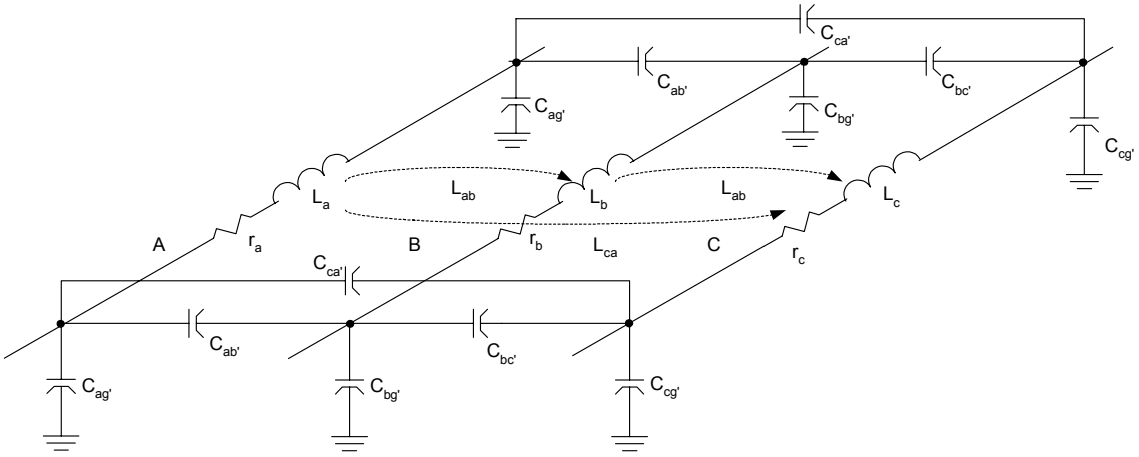

Figure 17 Transmission Line Π Equivalent Circuit

Figure 17 shows an equivalent Π circuit representing a transmission line section. If a transmission line lacks shunt reactors, we can simplify the equivalent circuit by considering only the electrostatic coupling of the phase conductors. Figure 18 represents a simplified, single, symmetrical, and fully transposed transmission line. The capacitances between phases are identical, i.e., $C_{ab} = C_{bc} = C_{ca} = C_m$ and the capacitances to ground for each phase are identical, i.e., $C_{ag} = C_{bg} = C_{cg} = C_g$.

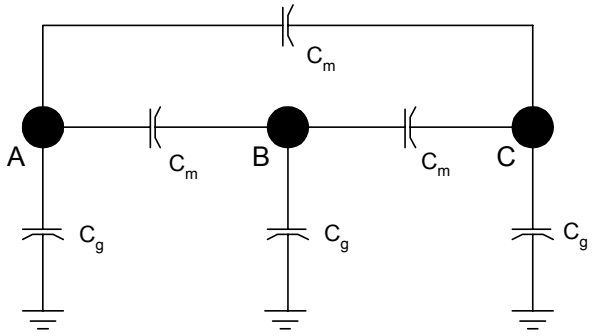

Figure 18 Equivalent Circuit Considering Only the Line Capacitances

If this system now experiences an A-phase-to-ground fault, we can represent the system during the pole-open condition as illustrated in Figure 19. This figure also shows the vector diagram while the secondary arc is present.

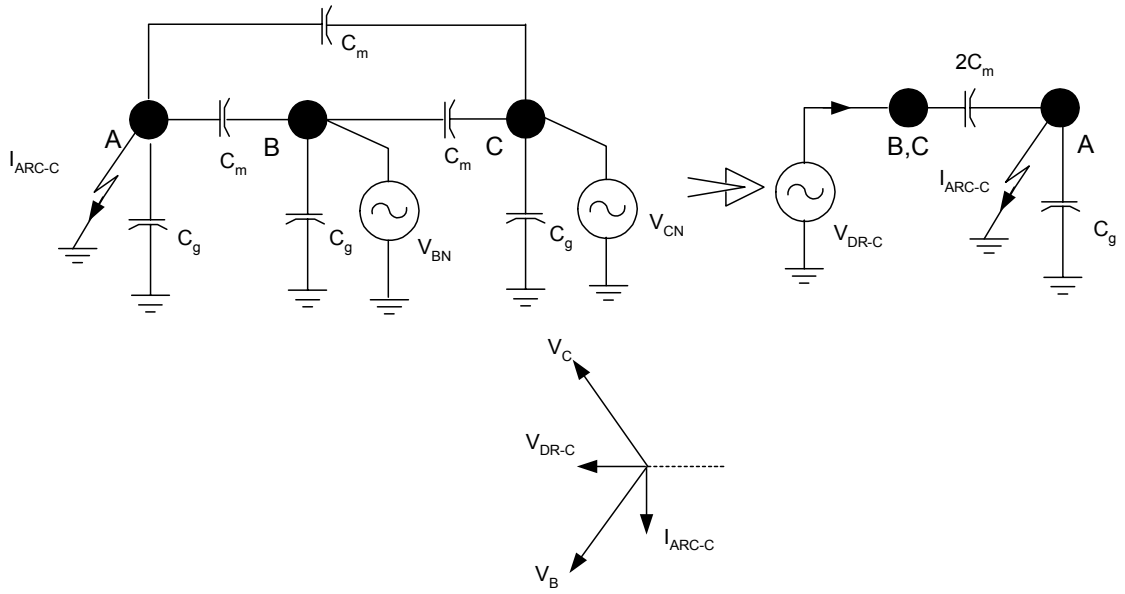

Figure 19 Equivalent Circuit While the Secondary Arc is Present

The magnitude of the secondary arc current resulting from the electrostatic coupling is a function of the line voltage and the line length. The line capacitance is a function of the distance between phase conductors and the height of these conductors above ground. If we represent the transmission line as a series of Π circuits, we can see that all these capacitances are effectively in parallel; the capacitance increases proportionally with the line length. From the equivalent circuit in Figure 19, we can calculate the secondary arc current, disregarding fault resistance, as follows:

$$I_{ARC-C} = V_{DR-C} \cdot j \cdot \varpi \cdot 2C_m \qquad \text{Equation 8}$$

Where the voltage V_{DR-C} for an A-phase-to-ground fault equals $(V_B + V_C)/2 = V_{LN}/2$. We can therefore rewrite Equation 8 as follows:

$$I_{ARC-C} = V_{LN} \cdot j \cdot \varpi \cdot C_m \qquad \text{Equation 9}$$

For a typical 400 kV line, I_{ARC-C} has an approximate value of 0.1085 A/km, or 10.85 A/ 100 km. Once the secondary arc extinguishes, a voltage known as the recovery voltage appears across the ground capacitance, C_g. The magnitude and/or rate of rise of the recovery voltage can initiate a re-strike. We can calculate the recovery voltage as follows:

$$V_{REC} = V_{LN} \cdot \frac{C_m}{(2C_m + C_g)} \qquad \text{Equation 10}$$

If the transmission line has shunt reactors, one must consider the electromagnetic coupling from the healthy phases; a portion of the secondary arc current becomes inductive. In this case, the secondary arc current is the vector sum of the electrostatic (I_{ARC-C}) and electromagnetic (I_{ARC-M}) currents. Calculation of the electromagnetic current is a non-trivial task; you would need the assistance of a transient analysis software package such as EMTP.

Secondary Arc Extinction Detectors, SAEDs

A secondary arc extinction detector can be added to supervise the closing signal to the breaker and prevent reclosing under fault. This supervision blocks the closing signal to the breaker when the secondary arc is present and minimizes the possibility of unsuccessful reclosures. Figure 20 shows the close supervision logic using secondary arc extinction detection (SAED) for close supervision. The SAED can minimize the dead time by initiating the reclose after the secondary arc extinguishes. The SAEDD time delay provides time for the air formerly occupied by the arc to regain dielectric capabilities.

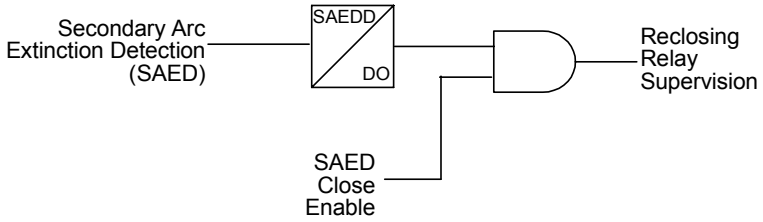

Figure 20 Reclosing Relay Close Supervision Using Secondary Arc Extinction Detection

Figure 21 shows the A-phase voltage after the line relay clears an A-phase-to-ground fault in an SPT application. After one pole opens, the voltage to ground, V_{ARC}, exists in the faulted phase until the secondary arc extinguishes. When the secondary arc extinguishes, a phase-to-ground voltage, V_A, results from the mutual coupling between the sound phases and the faulted phase. This voltage provides information to detect secondary arc extinction [18].

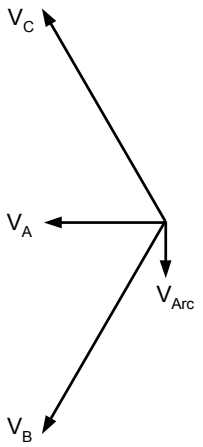

Figure 21 Line Voltages During the Pole-Open Condition

Complete reclosing relay supervision requires three secondary arc extinction detectors, one per phase. These detectors measure the angle, ϕ, between the phase-to-ground voltage of the faulted phase (V_γ) and the sum of the sound phases phase-to-ground voltages (V_Σ). For $-\beta \le \phi \le \beta$, and $|V_\gamma| > V_{thre}$, the detector determines the secondary arc extinction and asserts the SAED bit. β and V_{thre} determine the region that detects the secondary arc extinction. Table 3 shows the V_γ and V_Σ voltages for A-, B-, and C-phase SAEDs.

Table 3 V_γ and V_Σ Voltages for A-Phase, B-Phase, and C-Phase SAEDs

Detector	V_γ	V_Σ
A-phase	V_A	$V_B + V_C$
B-phase	V_B	$V_C + V_A$
C-phase	V_C	$V_A + V_B$

The angle $\phi = 180°$ and V_γ is outside of the SAED region when the line is energized under normal conditions as shown in Figure 22.

During single-pole open conditions, after the secondary arc extinguishes, the angle $\phi = 0°$ and V_γ is inside the SAED region (Figure 23). The A-phase detector asserts the SAED bit for this condition, allowing the reclosing sequence to continue.

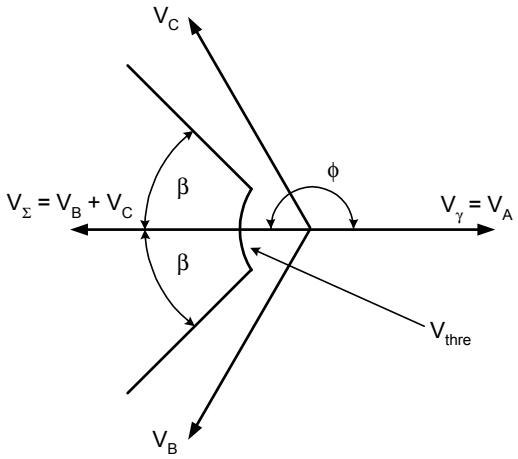

Figure 22 The Angle $\phi = 180°$ and V_γ is Outside of the SAED Region for Normal Conditions

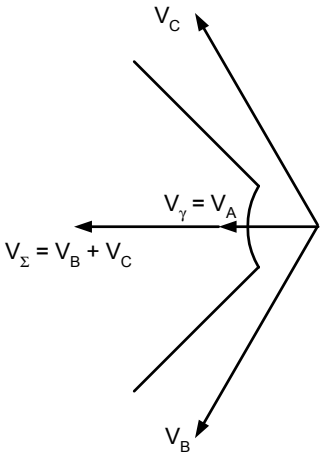

Figure 23 V_γ is Inside the SAED Region After the Arc Extinguishes

SAED Performance in Transmission Lines With Shunt Compensation

SAED is suitable for lines with or without shunt reactor compensation. We will look at the performance of the SAED for an A-phase-to-ground fault at the middle of the line in the power system shown in Figure 8. In this case, we assume that both breakers at the line ends open A-phase poles to create an A-phase open condition. Figure 24 shows the A-phase voltage and the fault current through the arc at the fault location. The fault occurs at cycle eight (133 ms) and the poles open at cycle 14 (233 ms). The figure also illustrates the presence of arc; primary arc exists before the breaker poles open, and secondary arc exists after the breakers clear the fault. The secondary arc extinguishes at cycle 23.5 (392 ms).

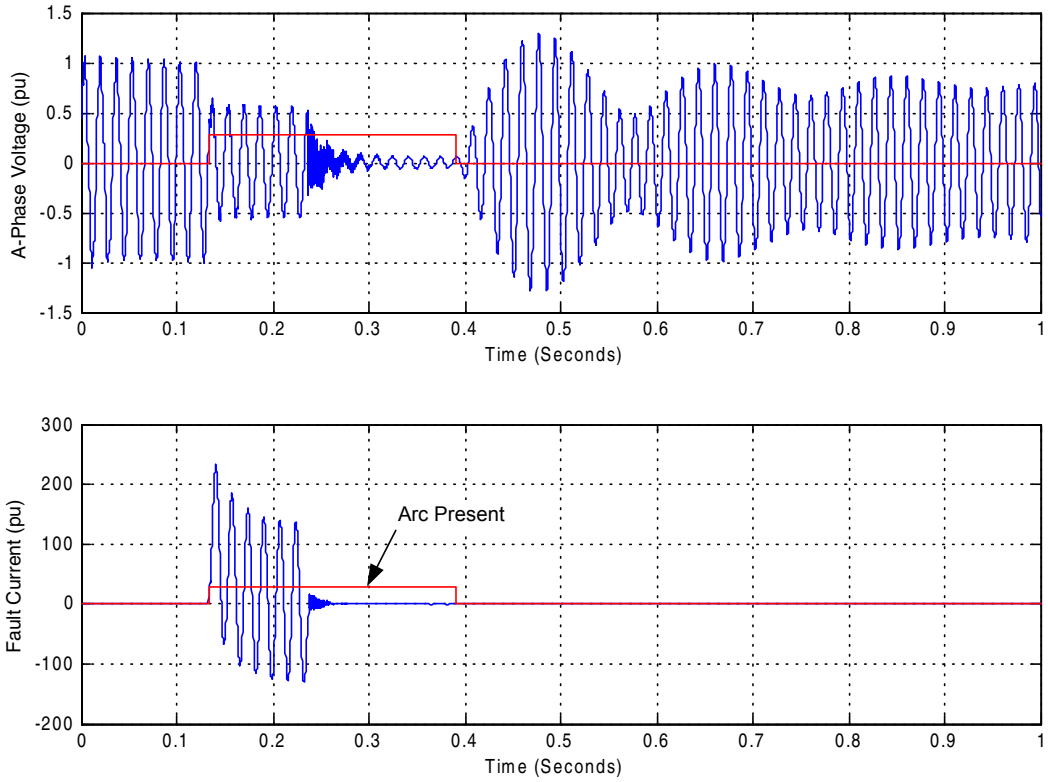

Figure 24 A-Phase Voltage, Arc Current, and Arc Presence Indication for an A-Phase-to-Ground Fault at the Middle of the Line

The A-phase voltage undergoes three significant changes during fault and pole-open conditions:

- Voltage reduction because of the fault presence. The voltage changes from normal to fault conditions.
- Additional voltage reduction after the breakers clear the fault. Reduced voltage exists during the pole-open condition while the secondary arc is present.
- Voltage increase during the pole-open condition. The voltage increases after the secondary arc extinguishes.

Figure 25 shows the A-phase voltage changes in magnitude and angle, and the SAED boundaries. During the pole-open condition before extinction of the secondary arc, the voltage magnitude is less than the voltage threshold, V_{thre}, and the voltage angle is outside the 2β angle limits. After the secondary arc extinguishes, the voltage magnitude exceeds the voltage threshold, V_{thre}, and the voltage angle is within the 2β angle limits of the SAED characteristic. You can see the A-phase voltage better in the polar plot of Figure 26. $V_A = 1\angle 0°$ (in per unit) before the fault occurs; $V_A = 0.7\angle 0°$ during the fault condition; $V_A = 0.1\angle 254°$ while the secondary arc is present; and $V_A = 0.8\angle 191°$ after the secondary arc extinguishes. The A-phase voltage operating point enters the A-phase SAED region after the secondary arc extinguishes.

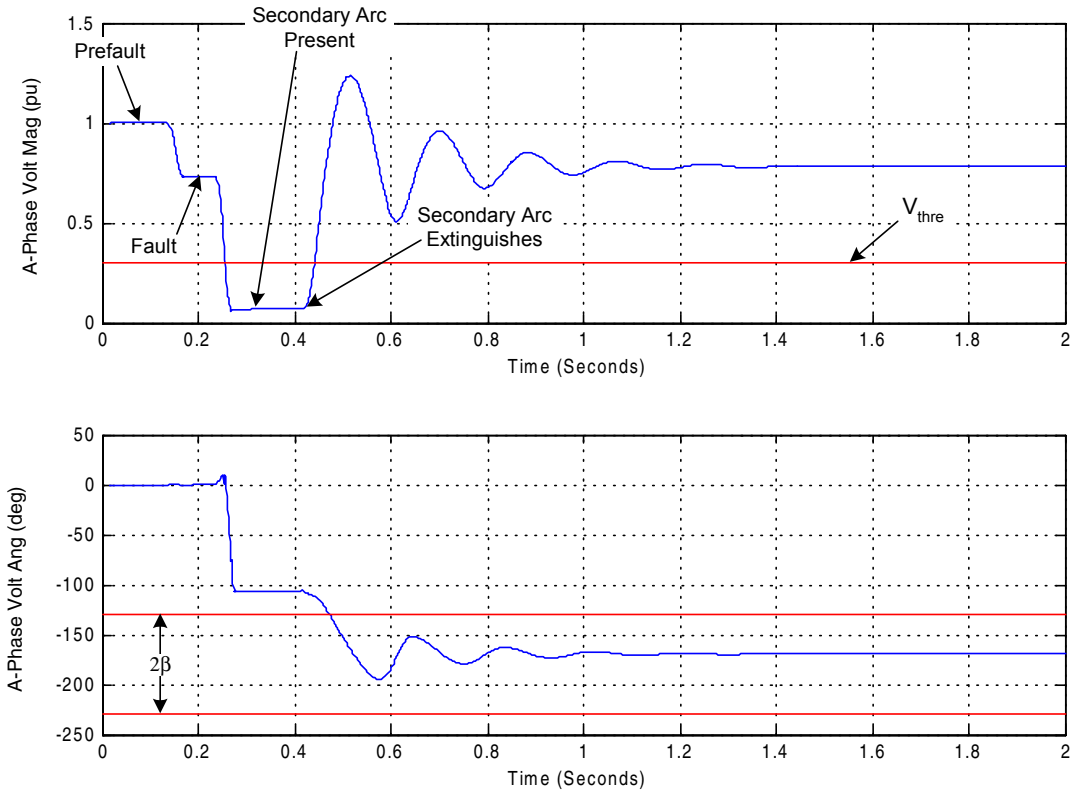

Figure 25 A-Phase Voltage Magnitude and Angle for an A-Phase-to-Ground Fault With the SAED Boundaries

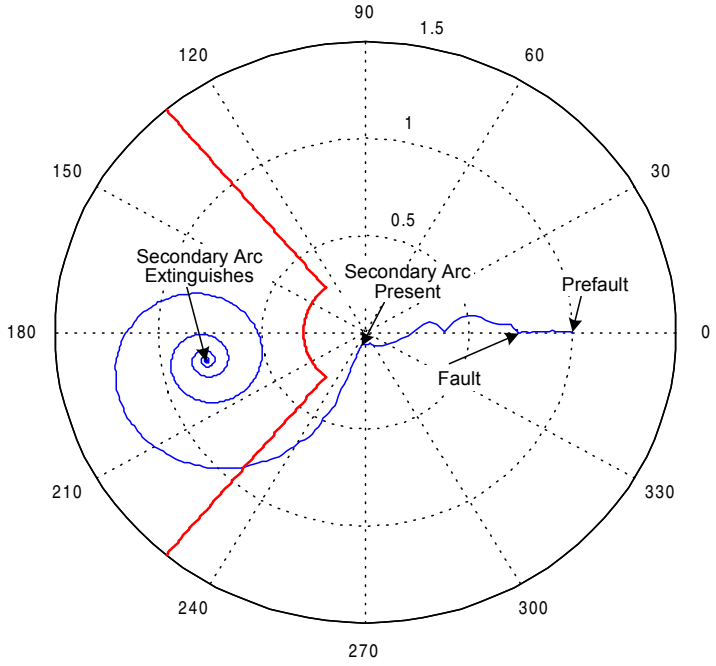

Figure 26 A-Phase Voltage Phasor Enters the SAED Characteristic After the Secondary Arc Extinguishes

CONCLUSIONS

1. The result of using the dual-filter scheme technique is reliable high-speed transmission line protection compared to conventional one-cycle only filtering schemes.

2. The ratio of the measured voltage, V_{MEAS}, to the calculated voltage, V_{CAL}, in series compensation applications provides information to block Zone 1 distance elements and prevent distance element overreach.

3. The ability to remove the open phase voltage prevents using corrupted signals for distance element polarization and frequency tracking during pole-open conditions or loss-of-potential conditions.

4. Using the composite signal, V_{α}, allows relays to track system frequency during pole-open conditions. The composite signal combines information from the three phases without additional signal manipulation, as in the case of positive-sequence quantity.

5. Secondary arc extinction detection prevents single-pole reclosing while the fault is present and optimizes the single pole-open interval, avoiding additional power system damage and minimizing system disturbance.

REFERENCES

[1] M. A. Adamiak, G. Alexander, and W. Premerlani "Advancements in Adaptive Algorithms for Secure High-Speed Protection," 23rd Annual Western Protective Relay Conference, Spokane, Washington, October 15–17, 1996.

[2] D. Hou, A. Guzman, and J. Roberts, "Inovative Solutions Improve Transmission Line Protection," 24th Western Protective Relay Conference, Spokane, WA, October 21–23, 1997.

[3] E. O. Schweitzer III and J. Roberts, "Distance Relay Element Design," 19th Annual Western Protective Relay Conference, Spokane, Washington, October 20–22, 1992.

[4] G. Benmouyal and J. Roberts, "Superimposed Quantities: Their True Nature and Their Application in Relays," Proceedings of the 26th Annual Western Protective Relay Conference, Spokane, WA, October 26–28, 1999.

[5] G. Benmouyal and J. Mahzeredjian, "A Combined Directional and Faulted Type Selector Element Based on Incremental Quantities," IEEE PES Summer Meeting 2001, Vancouver, Canada.

[6] A. Guzman, J. Roberts, and D. Hou, "New Ground Directional Elements Operate Reliably for Changing System Conditions," 23rd Annual Western Protective Relay Conference, Spokane, Washington, October 15–17, 1996.

[7] Instruction Manual for Digital Frequency Relay Model BE1-81 O/U, Basler Electric, Highland, Illinois. Publication: 9 1373 00 990. Revision: E. December 1992.

[8] A. G. Phadke and J. S. Thorp, "Computer Relaying for Power Systems," Research Studies Press Ltd. 1988.

[9] A. G. Phadke, J. S. Thorp, and M. G. Adamiak, "A New Measurement Technique for Tracking Voltage Phasors, Local System Frequency, and Rate of Change of Frequency," IEEE Transactions on Power Apparatus and Systems, Vol. PAS-102, No. 5, May 1983.

[10] P. J. Moore, J. H. Allmeling, and A. T. Johns, "Frequency Relaying Based on Instantaneous Frequency Measurement," IEEE/PES Winter Meeting, January 21–25, 1996, Baltimore, MD.

[11] IEEE PSRC Working Group: J. Esztergalyos et al. "Single-Phase Tripping and Auto Reclosing of Transmission Lines IEEE Committee Report."

[12] M. J. Pickett, H. L. Manning, and H. N. V. Geem, "Near Resonant Coupling on EHV Circuits: I-Field Investigations," IEEE Transactions on Power Systems, Vol. PAS-87, No. 2, February 1968.

[13] M. H. Hesse and D. D. Wilson, "Near Resonant Coupling on EHV Circuits: II-Method of Analysis," IEEE Transactions on Power Systems, Vol. PAS-87, No. 2, February 1968.

[14] E. Clarke, "Circuit Analysis of A-C Power Systems," General Electric, Schenectady, N.Y., 1950.

[15] C. F. Wagner and R. D. Evans, "Symmetrical Components as Applied to the Analysis of Unbalanced Electrical Circuits," McGraw-Hill, New York, 1933.

[16] D. L. Goldsworthy, "A Linearized Model for MOV-Protected Series Capacitors," IEEE Transactions on Power Systems, Vol. PWRS-2, No 4, Nov 1987, pp 953–958.

[17] E. N. Kimbark, "Suppression of Ground-Fault Arcs on Singe-Pole Switched EHV Lines by Shunt Reactors," IEEE Transactions on Power Apparatus and Systems, Vol. 83, March 1964.

[18] CFE-, LAPEM, UIE, ATN, "Secondary Arc Extinction Detection Project."

BIOGRAPHIES

Armando Guzmán, P.E. received his BSEE with honors from Guadalajara Autonomous University (UAG), Mexico, in 1979. He received a diploma in Fiber-Optics Engineering from Monterrey Institute of Technology and Advanced Studies (ITESM), Mexico, in 1990. He served as Regional Supervisor of the Protection Department in the Western Transmission Region of the Federal Electricity Commission (the electrical utility company of Mexico) for 13 years. He lectured at UAG in power system protection. Since 1993, he has been with Schweitzer Engineering Laboratories, Pullman, Washington, where he is presently a Research Engineer. He holds several patents in power system protection. He is a registered professional engineer in Mexico, is a senior member of IEEE, and has authored and coauthored several technical papers.

Joseph B. Mooney, P.E. received his B.Sc. in Electrical Engineering from Washington State University in 1985. He joined Pacific Gas and Electric Company upon graduation as a System Protection Engineer. In 1989, he left Pacific Gas and Electric and was employed by Bonneville Power Administration as a System Protection Maintenance District Supervisor. In 1991, he left Bonneville Power Administration and joined Schweitzer Engineering Laboratories as an Application Engineer. Shortly after starting with SEL, he was promoted to Application Engineering Manager. In 1999, he became Manager of the Power Engineering Group of the Research and Development department at Schweitzer Engineering Laboratories. He is a registered professional engineer in the states of California and Washington.

Gabriel Benmouyal, P.E. received his B.A.Sc. in Electrical Engineering and his M.A.Sc. in Control Engineering from Ecole Polytechnique, Université de Montréal, Canada in 1968 and 1970, respectively. In 1969, he joined Hydro-Québec as an Instrumentation And Control Specialist. He worked on different projects in the field of substation control systems and dispatching centers. In 1978, he joined IREQ, where his main field of activity was the application of microprocessors and digital techniques to substation and generating-station control and protection systems. In 1997, he joined Schweitzer Engineering Laboratories in the position of Research Engineer. He is a registered professional engineer in the Province of Québec, is an IEEE member, and has served on the Power System Relaying Committee since May 1989.

Normann Fischer joined Eskom as a Protection Technician in 1984. He received a Higher Diploma in Technology, with honors, from the Witwatersrand Technikon, Johannesburg, in 1988 and a B.Sc. in Electrical Engineering, with honors, from the University of Cape Town in 1993. He was a Senior Design Engineer in Eskom's Protection Design Department for three years, then joined IST Energy as a Senior Design Engineer in 1996. In 1999, he joined Schweitzer Engineering Laboratories as a Power Engineer in the Research and Development Division. He was a registered professional engineer in South Africa and a member of the South Africa Institute of Electrical Engineers.

Back to Table of Contents